International Journal of Heat and Mass Transfer 122 (2018) 631–642

Contents lists available at ScienceDirect

International Journal of Heat and Mass Transfer

journal homepage: www.elsevier.com/locate/ijhmt

A comparative study of local and nonlocal Allen-Cahn equations with mass conservation

Zhenhua Chai [a,b], Dongke Sun [c], Huili Wang [a], Baochang Shi [a,b,*]

[a] School of Mathematics and Statistics, Huazhong University of Science and Technology, Wuhan 430074, China
[b] Hubei Key Laboratory of Engineering Modeling and Scientific Computing, Huazhong University of Science and Technology, Wuhan 430074, China
[c] Jiangsu Key Laboratory for Design and Manufacture of Micro-Nano Biomedical Instruments, School of Mechanical Engineering, Southeast University, Nanjing 211189, China

ARTICLE INFO

Article history:
Received 8 October 2017
Received in revised form 25 December 2017
Accepted 4 February 2018
Available online 10 February 2018

Keywords:
Lattice Boltzmann model
Allen-Cahn equation
Chapman-Enskog analysis

ABSTRACT

The local and nonlocal Allen-Cahn equations (ACEs) have received increasing attention in the study of the complicated interfacial problems. In this paper, we conduct a comparison between local and nonlocal ACEs with the property of mass conservation in the framework of lattice Boltzmann (LB) method. To this end, we first propose two simple multiple-relaxation-time LB models for local and nonlocal ACEs, and through the Chapman-Enskog expansion, the local and nonlocal ACEs can be recovered correctly from the developed LB models. Then we test these two LB models with several examples, and the numerical results show that the developed LB models are accurate and also have a second-order convergence rate in space. Finally, a comparison between the local and nonlocal ACEs is also performed in terms of mass conservation, stability and accuracy. The results show that both local and nonlocal ACEs can preserve mass conservation of system and each phase. And additionally, it is also found that the local ACE is more accurate than nonlocal ACE in capturing the interface profile, but the latter is more stable than the former.

1. Introduction

The phase-field method, as one of interface capturing approaches, has gained a great success in the study of multiphase flows where the interfacial dynamics is of significant importance [1–5]. In this method, a diffusive interface with a finite width where the physical variables are smoothly distributed is assumed, and a phase-field variable or so-called order parameter governed by the Cahn-Hilliard equation (CHE) [6] or Allen-Cahn equation (ACE) [7] is also introduced to identify different phases. Usually, it is difficult to derive the analytical solutions of CHE and ACE, hence some numerical methods have been developed to solve the CHE and/or ACE in the past years [2,3,5], including finite-difference method [8–15], finite-element method [16,17], spectral method [12,18–20], and to name but a few. As an alternative to these traditional numerical methods, the lattice Boltzmann (LB) method can also be used to solve the CHE and ACE that are considered as the special cases of nonlinear convection-diffusion equation [21–35]. Based on the fact that the CHE can conserve the mass of multiphase system, while the ACE cannot, most of the works based on LB method mainly focused on the CHE [21–31]. However, from the theoretical point of view, the CHE is a fourth-order partial differential equation, and through the Chapman-Enskog analysis, it cannot be directly recovered from the LB models. Furthermore, it is also found that in the CHE, the drop would eventually disappear if its radius is smaller than a critical value [36,37]. On the other hand, from the numerical point of view, the most appealing property, i.e., locality of collision process, cannot be preserved in the LB models for CHE since the nonlocal finite-difference schemes are needed to calculate space derivatives of order parameter [21–31]. To solve above problems inherent in the LB models for CHE, Geier et al. [32] proposed a LB model for the local ACE with mass conservation [38,39], and found that the results of LB models for local ACE and CHE are comparable, but the model for ACE has a higher-order convergence rate in space. Based on this work, they further presented a simple LB model for the ACE in three-dimensional space [33]. However, as pointed out by Ren et al. [34], through the Chapman-Enskog analysis, it can be found that the LB models in Refs. [32,33] cannot give the correct local ACE. To overcome the drawback, Ren et al. [34] proposed an improved multiple-relaxation-time (MRT) LB model for the same ACE, and found that the ACE can be recovered correctly through the Chapman-Enskog analysis. Almost at the same time, Wang et al. [35] also independently developed a new

* Corresponding authors at: School of Mathematics and Statistics, Huazhong University of Science and Technology, Wuhan 430074, China.
E-mail addresses: hustczh@hust.edu.cn (Z. Chai), shibc@hust.edu.cn (B. Shi).

https://doi.org/10.1016/j.ijheatmasstransfer.2018.02.013
0017-9310/

LB model for ACE which can be viewed as a single-relaxation-time version of the model in Ref. [34]. Then they also performed a comparative study on the LB models for ACE and CHE, and the results show that although the results of these two LB models are comparable, the model for ACE is much simpler and more stable. Nevertheless, we would like to point out that in these available LB models for local ACE, some gradient terms of order parameter are also included, and usually there are two popular ways that can be used to calculate these gradient terms. The first is *local* method where the gradient terms are computed locally through moments of non-equilibrium distribution function [32,33,35]. Although this method can ensure that the collision process is implemented locally, it may decrease the accuracy of LB models [32]. The second is *nonlocal* method in which the finite-difference scheme is applied for the gradient terms [32–34]. This method could be used to improve the accuracy of LB model for local ACE [32], but the locality of collision process cannot be guaranteed.

On the other hand, to overcome the shortcoming of original ACE in preserving mass conservation [7], the nonlocal ACEs with different Lagrange multipliers are also developed [11,40,41]. Rubinstein and Sternberg [40] first presented a nonlocal ACE with a time-dependent Lagrange multiplier, and later this nonlocal ACE is also used to study two-phase flows [42,43]. However, as reported in Refs. [11,41], the nonlocal ACE proposed by Rubinstein and Sternberg can only conserve mass up to order ε which is a small parameter related to interface width, and cannot preserve the small features of system. To solve the problem, Brassel and Bretin [41] developed another nonlocal ACE with a modified Lagrange multiplier, and through the theoretical and numerical analysis, they found that this ACE can preserve the mass of system up to ε^2. Kim et al. also performed some numerical studies on the nonlocal ACEs [11], and conducted a comparison between the ACEs and CHEs [14]. The results in their works show that the nonlocal ACE proposed Brassel and Bretin can preserve the small features accurately. Recently, they further extended their previous works, and considered the Allen-Cahn-Navier-Stokes system for incompressible two-phase flows [44].

From above review and discussion, one can find that both the local and nonlocal ACEs can be used to depict the interface between different phases, and more complex two-phase fluid flows when they couple with the Navier-Stokes equations. However, the advantages and/or disadvantages of local and nonlocal ACEs in preserving mass conservation, depicting interface profile and capturing small features are unclear. In this work, we would perform a comparative study of the local and nonlocal ACEs in the framework of LB method, but for simplicity, the effect of velocity governed by the Navier-Stokes equations is not considered here.

The rest of the paper is organized as follows. In Section 2, the local and nonlocal ACEs with mass conservation are first introduced, then two simple LB models for local and nonlocal ACEs are proposed in Section 3. In Section 4, we present some numerical results and discussion, and finally, some conclusions are given in Section 5.

2. Local and nonlocal ACEs with mass conservation

In the phase-field theory, the free energy density of a system can be simply written as [2,8,10]

$$f(\phi,\ \nabla\phi) = \frac{1}{2}|\nabla\phi|^2 + \psi(\phi). \tag{1}$$

It is clear that the free energy density defined by Eq. (1) includes two parts: the first term is gradient energy, and the second term $\psi(\phi)$ is bulk energy with two minima for a two-phase system. Usually, the bulk energy can be approximated by [2,10]

$$\psi(\phi) = \frac{1}{4\epsilon^2}(\phi^2-1)^2, \tag{2}$$

where ϵ is capillary width, which is also related to thickness of diffusive interface. ϕ is order parameter, and can be used to label different phases with different values,

$$\phi = \begin{cases} 1, & \text{phase 1}, \\ -1, & \text{phase 2}. \end{cases} \tag{3}$$

The interface Γ between two different phases can be described by the zero level set of order parameter $\Gamma = \{\mathbf{x} \in \Omega | \phi(\mathbf{x},\ t) = 0\}$.

Based on the free energy density mentioned above, one can also define the mixing energy F and chemical potential μ,

$$F(\phi,\ \nabla\phi) = \int_\Omega f(\phi,\ \nabla\phi)d\Omega = \int_\Omega \left[\psi(\phi) + \frac{1}{2}|\nabla\phi|^2\right]d\Omega, \tag{4}$$

$$\mu = \frac{\delta F}{\delta\phi} = \psi'(\phi) - \nabla^2\phi = \frac{\phi(\phi^2-1)}{\epsilon^2} - \nabla^2\phi, \tag{5}$$

where Ω is the physical domain occupied by the system, ψ' is the derivative of function ψ with respect to ϕ. When the diffusive interface is at equilibrium, the chemical potential is zero, and one can obtain the solution of ϕ under condition of $\phi(x_0) = 0$,

$$\phi(x_n) = \tanh\left(\frac{x_n - x_0}{\sqrt{2}\epsilon}\right), \tag{6}$$

where x_n is the spatial variable normal to interface located at x_0.

2.1. Local ACE with mass conservation

Based on the previous work [38], the interface advection equation can be written as

$$\phi_t + u_n\mathbf{n}\cdot\nabla\phi = 0, \tag{7}$$

where $\mathbf{n}$ and u_n are the unit normal vector and normal interface speed, and can be given by

$$\mathbf{n} = \frac{\nabla\phi}{|\nabla\phi|},\quad u_n = -M_\phi\kappa. \tag{8}$$

M_ϕ is a positive constant, and is also named mobility. κ is the interface curvature, and can be expressed as

$$\kappa = \nabla\cdot\mathbf{n} = \nabla\cdot\left(\frac{\nabla\phi}{|\nabla\phi|}\right) = \frac{1}{|\nabla\phi|}\left[\nabla^2\phi - \frac{(\nabla\phi\cdot\nabla)|\nabla\phi|}{|\nabla\phi|}\right]. \tag{9}$$

With the equilibrium distribution defined by Eq. (6), the gradient of ϕ and its normal can be determined by

$$|\nabla\phi| = \frac{\partial\phi}{\partial x_n} = \frac{1-\phi^2}{\sqrt{2}\epsilon},\quad \frac{(\nabla\phi\cdot\nabla)|\nabla\phi|}{|\nabla\phi|} = -\frac{\phi(1-\phi^2)}{\epsilon^2}. \tag{10}$$

Substituting Eq. (10) into Eq. (9), we can derive expression of curvature,

$$\kappa = \frac{1}{|\nabla\phi|}\left[\nabla^2\phi + \frac{\phi(1-\phi^2)}{\epsilon^2}\right]. \tag{11}$$

With the help Eqs. (8) and (11), one can rewrite Eq. (7) as

$$\phi_t = M_\phi\left[\nabla^2\phi + \frac{\phi(1-\phi^2)}{\epsilon^2}\right]. \tag{12}$$

To describe the case of no curvature-driven interface motion [38,39], the counter term approach introduced by Folch et al. [45] is adopted, and consequently, Eq. (12) can be modified by

$$\phi_t = M_\phi\left[\nabla^2\phi + \frac{\phi(1-\phi^2)}{\epsilon^2} - |\nabla\phi|\nabla\cdot\left(\frac{\nabla\phi}{|\nabla\phi|}\right)\right]. \tag{13}$$

Then following the procedure in Ref. [39], Eq. (13) can also be reformulated in a conservative form,

$$\phi_t = M_\phi\left[\nabla^2\phi - \nabla\cdot\left(\frac{1-\phi^2}{\sqrt{2}\epsilon}\frac{\nabla\phi}{|\nabla\phi|}\right)\right] = M_\phi\nabla\cdot\left[\left(1-\frac{1-\phi^2}{\sqrt{2}\epsilon}\frac{1}{|\nabla\phi|}\right)\nabla\phi\right], \tag{14}$$

which is considered as the local ACE, and can also be obtained with the approach shown in Ref. [32]. In addition, we can also show that Eq. (14) can enforce the mass conservation of system under natural boundary condition ($\mathbf{n}\cdot\nabla\phi = 0$),

$$\frac{d}{dt}\int_\Omega \phi d\mathbf{x} = \int_\Omega \phi_t d\mathbf{x} = M_\phi\int_\Omega \nabla\cdot\left[\left(1-\frac{1-\phi^2}{\sqrt{2}\epsilon}\frac{1}{|\nabla\phi|}\right)\nabla\phi\right]d\mathbf{x} = M_\phi\int_{\partial\Omega}\mathbf{n}\cdot\left[\nabla\phi\left(1-\frac{1-\phi^2}{\sqrt{2}\epsilon}\frac{1}{|\nabla\phi|}\right)\right]dS = 0. \tag{15}$$

2.2. Nonlocal ACE with mass conservation

It is known that in the phase-field theory, the dynamics of the order parameter ϕ can be determined by the gradient flow [2],

$$\phi_t = -M_\phi\frac{\delta F}{\delta\phi}. \tag{16}$$

If we take the variational derivative $\delta F/\delta\phi$ in L^2 space, the following ACE can be obtained,

$$\phi_t = M_\phi(\nabla^2\phi - \psi'). \tag{17}$$

Here it should be noted that this classical ACE (17) cannot conserve the mass of system under the natural boundary condition ($\mathbf{n}\cdot\nabla\phi = 0$), which can be seen clearly through the following equation,

$$\frac{d}{dt}\int_\Omega \phi d\mathbf{x} = \int_\Omega \phi_t d\mathbf{x} = M_\phi\int_\Omega(\nabla^2\phi - \psi')d\mathbf{x} = M_\phi\int_{\partial\Omega}\mathbf{n}\cdot\nabla\phi dS - M_\phi\int_\Omega\psi' d\mathbf{x} = -M_\phi\int_\Omega\psi' d\mathbf{x}, \tag{18}$$

which is not always zero. To overcome this problem, Rubinstein and Sternberg [40] developed another ACE through introducing a nonlocal Lagrange multiplier $\beta(t)$ into the classical ACE,

$$\phi_t = M_\phi\left[\nabla^2\phi - \psi' + \beta(t)\right], \tag{19}$$

where the Lagrange multiplier $\beta(t)$ is defined by

$$\beta(t) = \frac{\int_\Omega\psi' d\mathbf{x}}{\int_\Omega d\mathbf{x}}. \tag{20}$$

Based on above definition of the Lagrange multiplier $\beta(t)$, one can show that Eq. (19) satisfies the condition of mass conservation, i.e.,

$$\frac{d}{dt}\int_\Omega\phi d\mathbf{x} = 0. \tag{21}$$

We noted that Eq. (19) is also called the conservative and nonlocal ACE [2,11]. Although this conservative ACE has been adopted to study some two-phase problems [42,43], it also has a drawback in preserving small features since the Lagrange multiplier is only a function of time [11,41]. Actually, similar to results of CHE [36,37], if the radius of drop is less than a critical value, the drop would also eventually disappear [11,14]. To improve the capacities of ACE in capturing small features and preserving mass conservation, Brassel and Bretin proposed a modified conservative and nonlocal ACE [41],

$$\phi_t = M_\phi\left[\nabla^2\phi - \psi' + \beta(t)\sqrt{2\psi}\right] = M_\phi\left[\nabla^2\phi + \frac{\phi(1-\phi^2)}{\epsilon^2} + \beta(t)\sqrt{2\psi}\right], \tag{22}$$

where the Lagrange multiplier $\beta(t)$ is redefined by

$$\beta(t) = \frac{\int_\Omega\psi' d\mathbf{x}}{\int_\Omega\sqrt{2\psi}d\mathbf{x}}. \tag{23}$$

Compared to Eq. (19), this improved nonlocal ACE (22) not only can capture small features of system [11], but also can ensure that the conservation of the mass contains both nonlocal and local effects [46]. For this reason, we will only consider the nonlocal ACE (22) in this work.

Finally, we would also like to point out that although the local and nonlocal ACEs are obtained from different points of view (see Eqs. (13) and (22)), they are almost the same except the last terms in right sides of Eqs. (13) and (22), which are used to preserve the mass conservation of system.

3. LB models for local and nonlocal ACEs

In the past decades, the LB method, as a mesoscopic numerical approach, has gained a great success in the study of complex fluid flows [47–53] and physical systems governed by some particular partial differential equations [54–56]. Historically, the LB method originated from the lattice gas automata [57], but later it is also shown that this method can also be viewed as a special discrete form of the continuous Boltzmann equation [58]. Based on the collision term, the models of LB method can be classified into three kinds, i.e., the single-relaxation-time LB model (or so-called lattice BGK model) [59], the two-relaxation-time LB model [54,60], and the multiple-relaxation-time (MRT) LB model (or the generalized LB model) [61,62]. In this work, we will consider the MRT LB model for its numerical stability and accuracy in the study of fluid flows [25,63,64] and convection-diffusion equations [65–67].

The evolution equation of MRT LB model can be written as [49,56,61,62,68]

$$f_i(\mathbf{x}+\mathbf{c}_i\delta t,\ t+\delta t) = f_i(\mathbf{x},\ t) - (\mathbf{M}^{-1}\mathbf{S}\mathbf{M})_{ij}\left[f_j(\mathbf{x},\ t) - f_j^{(eq)}(\mathbf{x},\ t)\right] + \delta t R_i(\mathbf{x},\ t),\ i = 0,\ 1,\ \ldots,\ q-1, \tag{24}$$

where $f_i(\mathbf{x},\ t)$ is the distribution function associated with the discrete velocity $\mathbf{c}_i$ at position $\mathbf{x}$ and time t, q is the number of discrete velocity directions. $\mathbf{M}$ is the transformation matrix, R_i is the discrete source term. $f_i^{(eq)}(\mathbf{x},\ t)$ is the equilibrium distribution function, and can be expressed as

$$f_i^{(eq)}(\mathbf{x},\ t) = \omega_i\phi, \tag{25}$$

where ω_i is the weight coefficient. In some commonly used DdQq (q velocities in d dimensional space) lattice models, the weight coefficient ω_i and discrete velocity $\mathbf{c}_i$ are defined by [49,50,59,65,67]

D1Q2:

$$\omega_1 = \omega_2 = \frac{1}{2}, \tag{26a}$$

$$\mathbf{c} = (1,-1)c, \tag{26b}$$

D1Q3:

$$\left\{\omega_0 = \frac{2}{3},\ \omega_1 = \omega_2 = \frac{1}{6}\right\}\ \text{or}\ \left\{\omega_{i=0-2} = \frac{1}{3}\right\} \tag{27a}$$

$$\mathbf{c} = (0,1,-1)c, \tag{27b}$$

D2Q4:

$$\omega_{i=1-4}=\frac{1}{4}, \tag{28a}$$

$$\mathbf{c}=\begin{pmatrix}1 & 0 & -1 & 0\\ 0 & 1 & 0 & -1\end{pmatrix}c, \tag{28b}$$

D2Q5:

$$\left\{\omega_0=\frac{1}{3},\ \omega_{i=1-4}=\frac{1}{6}\right\}\ \text{or}\ \left\{\omega_{i=0-4}=\frac{1}{5}\right\}, \tag{29a}$$

$$\mathbf{c}=\begin{pmatrix}0 & 1 & 0 & -1 & 0\\ 0 & 0 & 1 & 0 & -1\end{pmatrix}c, \tag{29b}$$

D2Q9:

$$\omega_0=\frac{4}{9},\ \omega_{i=1-4}=\frac{1}{9},\ \omega_{i=5-8}=\frac{1}{36}, \tag{30a}$$

$$\mathbf{c}=\begin{pmatrix}0 & 1 & 0 & -1 & 0 & 1 & -1 & -1 & 1\\ 0 & 0 & 1 & 0 & -1 & 1 & 1 & -1 & -1\end{pmatrix}c, \tag{30b}$$

D3Q6:

$$\omega_{i=1-6}=\frac{1}{6}, \tag{31a}$$

$$\mathbf{c}=\begin{pmatrix}1 & -1 & 0 & 0 & 0 & 0\\ 0 & 0 & 1 & -1 & 0 & 0\\ 0 & 0 & 0 & 0 & 1 & -1\end{pmatrix}c, \tag{31b}$$

D3Q7:

$$\left\{\omega_0=\frac{1}{4},\ \omega_{i=1-6}=\frac{1}{8}\right\}\ \text{or}\ \left\{\omega_{i=0-6}=\frac{1}{7}\right\}, \tag{32a}$$

$$\mathbf{c}=\begin{pmatrix}0 & 1 & -1 & 0 & 0 & 0 & 0\\ 0 & 0 & 0 & 1 & -1 & 0 & 0\\ 0 & 0 & 0 & 0 & 0 & 1 & -1\end{pmatrix}c, \tag{32b}$$

D3Q15:

$$\omega_0=\frac{2}{9},\ \omega_{i=1-6}=\frac{1}{9},\ \omega_{i=7-14}=\frac{1}{72}, \tag{33a}$$

$$\mathbf{c}=\begin{pmatrix}0 & 1 & -1 & 0 & 0 & 0 & 0 & 1 & 1 & 1 & 1 & -1 & -1 & -1 & -1\\ 0 & 0 & 0 & 1 & -1 & 0 & 0 & 1 & -1 & -1 & 1 & 1 & -1 & -1 & 1\\ 0 & 0 & 0 & 0 & 0 & 1 & -1 & 1 & -1 & 1 & -1 & 1 & -1 & 1 & -1\end{pmatrix}c, \tag{33b}$$

where $c=\delta x/\delta t$ with δx and δt representing lattice spacing and time step, respectively. In the MRT LB model, $\mathbf{M}$ is a $q\times q$ matrix that transforms the distribution function f_i, equilibrium distribution function $f_i^{(eq)}$ and discrete source term R_i to their moments,

$$\mathbf{m}:=\mathbf{M}\mathbf{f},\quad \mathbf{m}^{(eq)}:=\mathbf{M}\mathbf{f}^{(eq)},\quad \mathbf{Q}:=\mathbf{M}\mathbf{R}, \tag{34}$$

where $\mathbf{f}=(f_0,f_1,\ldots,f_{q-1})^{\top},\mathbf{f}^{(eq)}=(f_0^{(eq)},f_1^{(eq)},\ldots,f_{q-1}^{(eq)})^{\top},\mathbf{R}=(R_0,R_1,\ldots,R_{q-1})^{\top}$, $\top$ denotes the transpose of a matrix. $\mathbf{S}=\mathrm{diag}(s_0,s_1,\ldots,s_{q-1})$ is a diagonal relaxation matrix, and s_i is non-negative relaxation parameter corresponding to the ith moment of distribution function.

For simplicity but without losing generality, in this work, we only consider the simple D2Q4 lattice model for two-dimensional local and nonlocal ACEs that can be viewed as a special diffusion equation with a source term. In this lattice model, the transformation matrix $\mathbf{M}$ and relaxation matrix $\mathbf{S}$ can be given by [65,66]

$$\mathbf{M}=\mathbf{C}_d\mathbf{M}_0,\ \mathbf{C}_d=\mathrm{diag}(1,c,c,c^2),\quad \mathbf{M}_0=\begin{pmatrix}1 & 1 & 1 & 1\\ 1 & 0 & -1 & 0\\ 0 & 1 & 0 & -1\\ 1 & -1 & 1 & -1\end{pmatrix}, \tag{35a}$$

$$\mathbf{S}=\mathrm{diag}(s_0,\ s_1,\ s_1,\ s_2). \tag{35b}$$

It should be noted that in Eq. (35b), the second and third elements of relaxation matrix $\mathbf{S}$ are labeled by the same parameter s_1 since both of them correspond to the first-order moment of distribution function, and similarly, the fourth relaxation parameter denoted by s_2 corresponds to the second-order moment of distribution function. Actually, it is also known that if all relaxation parameters s_i $(i=0-2)$ are identical to each other, the MRT LB model will reduce to the lattice BGK model.

In addition, based on Eq. (35a), one can obtain the following relation,

$$\mathbf{M}_0^{-1}\mathbf{S}\mathbf{M}_0=\mathbf{M}^{-1}\mathbf{S}\mathbf{M}, \tag{36}$$

then the evolution equation of MRT LB model can be rewritten as

$$f_i(\mathbf{x}+\mathbf{c}_i\delta t,\ t+\delta t)=f_i(\mathbf{x},\ t)-(\mathbf{M}_0^{-1}\mathbf{S}\mathbf{M}_0)_{ij}\left[f_j(\mathbf{x},\ t)-f_j^{(eq)}(\mathbf{x},\ t)\right]+\delta t R_i(\mathbf{x},\ t),\ i=0,\ 1,\ \ldots,\ q-1. \tag{37}$$

Now we would like to give two remarks on above MRT LB model.

Remark I. The evolution of the MRT LB model consists of two steps, i.e., collision and streaming [61],

$$\text{Collision}:\ \mathbf{m}^{+}(\mathbf{x},\ t)=\mathbf{m}(\mathbf{x},\ t)-\mathbf{S}[\mathbf{m}(\mathbf{x},\ t)-\mathbf{m}^{(eq)}(\mathbf{x},\ t)]+\delta t\mathbf{Q}, \tag{38a}$$

$$\text{Streaming}: f_i(\mathbf{x}+\mathbf{c}_i\delta t,t+\delta t)=f_i^{+}(\mathbf{x},t),\quad f_i^{+}(\mathbf{x},t)=\mathbf{M}_{ij}^{-1}\mathbf{m}_j^{+}(\mathbf{x},t), \tag{38b}$$

where $f_i^{+}(\mathbf{x},\ t)$ is the post-collision distribution function. In addition, it can also be found that the same as lattice BGK model, the streaming process of MRT LB model is still conducted in velocity space, but unlike the lattice BGK model, the collision process of MRT LB model is implemented in moment space.

Remark II. Compared to the lattice BGK model, the MRT LB model possesses more relaxation parameters that can be adjusted to improve its numerical accuracy and stability [62,64–66]. Based on the results reported in some previous works [49,65,66], the relaxation parameter s_0 corresponding to zero-order moment or the conservation variable almost has no effect on the derivation of macroscopic equation, the accuracy and stability of MRT LB model. For this reason, $s_0=0$ is usually adopted in the MRT LB models, and would also be used in the following numerical simulations. On the contrary, the relaxation parameter s_2 corresponding to the second-order moment has a significant influence on the accuracy of MRT LB model, and based on some recent results [65,66], $s_2=2-s_1$ is applied in this work.

3.1. LB model for local ACE

Although there are some LB models for two-dimensional local ACE in which the D2Q5 and D2Q9 lattices are adopted [32,34,35], in this part we would present a more efficient LB model with D2Q4 lattice. Based on the previous works [34,35], the evolution equation of MRT LB model for local ACE reads

$$f_i(\mathbf{x}+\mathbf{c}_i\delta t, t+\delta t) = f_i(\mathbf{x}, t) - (\mathbf{M}^{-1}\mathbf{S}\mathbf{M})_{ij}\left[f_j(\mathbf{x}, t) - f_j^{(eq)}(\mathbf{x}, t)\right] + \delta t\left[\mathbf{M}^{-1}\left(\mathbf{I}-\frac{\mathbf{S}}{2}\right)\mathbf{M}\right]_{ij}\omega_j\mathbf{c}_j\cdot\left(\frac{1-\phi^2}{\sqrt{2}\epsilon}\frac{\nabla\phi}{|\nabla\phi|}\right), i=1, 2, 3, 4. \quad (39)$$

where $\mathbf{I}$ is the unit matrix. The order parameter ϕ can be computed through a summation of the distribution function,

$$\phi(\mathbf{x}, t) = \sum_{i=1}^{4} f_i(\mathbf{x}, t). \quad (40)$$

In addition, following some previous works [35,68,69], a local scheme for gradient term is developed to ensure that the collision process of MRT LB can be performed locally (see some details in Appendix A),

$$\nabla\phi = -\frac{4}{\delta t c^2}(m_1, m_2)^{\top} = -\frac{4}{\delta t c^2}\sum_i \mathbf{c}_i f_i, \quad (41)$$

then one can also obtain the normal of $\nabla\phi$,

$$|\nabla\phi| = \frac{4}{\delta t c^2}\left|\sum_i \mathbf{c}_i f_i\right|. \quad (42)$$

3.2. LB model for nonlocal ACE

For the nonlocal ACE, the evolution equation of MRT LB model with D2Q4 lattice can be expressed as

$$f_i(\mathbf{x}+\mathbf{c}_i\delta t, t+\delta t) = f_i(\mathbf{x}, t) - (\mathbf{M}^{-1}\mathbf{S}\mathbf{M})_{ij}\left[f_j(\mathbf{x}, t) - f_j^{(eq)}(\mathbf{x}, t)\right] + \delta t\left[\mathbf{M}^{-1}\left(\mathbf{I}-\frac{\mathbf{S}}{2}\right)\mathbf{M}\right]_{ij}\omega_j R, \; i=1, 2, 3, 4, \quad (43)$$

where R is the source term,

$$R = M_\phi\left[\frac{\phi(1-\phi^2)}{\epsilon^2} + \beta(t)\sqrt{2}\psi\right]. \quad (44)$$

Unlike Eq. (40), the order parameter ϕ in this model should be calculated by

$$\phi(\mathbf{x}, t) = \sum_{i=1}^{4} f_i(\mathbf{x}, t) + \frac{\delta t}{2}R. \quad (45)$$

Through the Chapman-Enskog analysis (see Appendixes A and B), the local and nonlocal ACEs can be recovered from the MRT-LB models with the following mobility M_ϕ,

$$M_\phi = \frac{1}{2}\left(\frac{1}{s_1}-\frac{1}{2}\right)\frac{\delta x^2}{\delta t}. \quad (46)$$

4. Numerical results and discussion

In this section, we would carry out some simulations to give a comparison between local and nonlocal ACEs in describing evolution of two-dimensional disks, and mainly focus on the interface profile, the mass conservation of phase 1, phase 2 and system, the maximum and minimum values of order parameter ϕ. Similar to the discussion in some previous works [3,11,38], when the value of equilibrium order parameter (see Eq. (6)) is varied from -0.9 to 0.9, the corresponding distance across interface is $2\sqrt{2}\epsilon\tanh^{-1}(0.9)$. If the distance is approximated by m lattice spacings, one can determine the value of ϵ,

$$\epsilon = \frac{m\delta x}{2\sqrt{2}\tanh^{-1}(0.9)}. \quad (47)$$

In the following simulations, ϵ would be fixed to be 0.015, and unless otherwise stated, the periodic boundary condition would also be adopted.

In addition, to measure difference between the numerical and analytical results, the following relative error is adopted,

$$E = \frac{\sum_{(x, y)}|\phi_a(x, y) - \phi_n(x, y)|}{\sum_{(x, y)}|\phi_a(x, y)|}, \quad (48)$$

where ϕ_a and ϕ_n are analytical and numerical solutions.

4.1. Evolution of a static disk

We first consider a simple periodic problem, i.e., evolution of a static disk placed in the center of physical domain $\Omega = [0, 1]\times[0, 1]$ with the following initial condition,

$$\phi(x, y, 0) = \tanh\frac{R - \sqrt{(x-0.5)^2 + (y-0.5)^2}}{\sqrt{2}\epsilon}, \quad (49)$$

where the radius of disk (R) is fixed to be 0.25. Similar to the discussion in some previous works [24,26,27], for a relatively large R, the initial solution (49) can be considered as an approximate analytical solution, and is also denoted as $\phi_a(x, y)$ appeared in Eq. (48).

We performed some simulations with the mobility $M_\phi = 0.001$, the relaxation parameter $s_1 = 1.25$ and the lattice size 128×128 ($m = 8$), and presented numerical results of interface profile in Fig. 1. As seen from this figure, the local and nonlocal ACEs almost give the same results, and these results are also in good agreement with the initial solution. To give a quantitative comparison between the local and nonlocal ACEs, we also measured the rela-

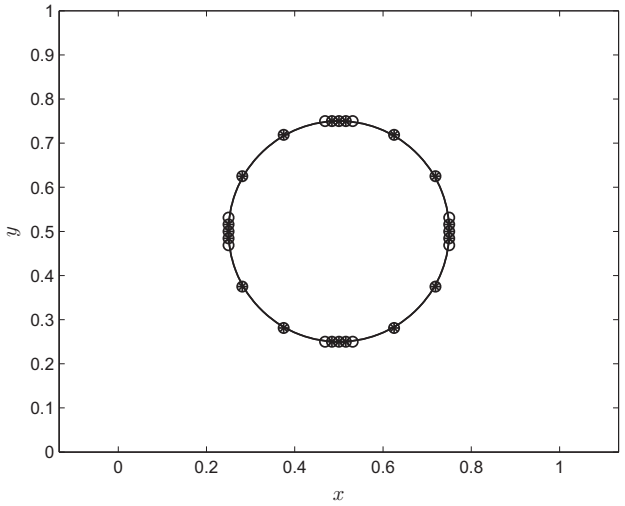

Fig. 1. The interface profile of static disk [solid line: initial profile defined by Eq. (49), ○: local ACE, ∗: nonlocal ACE].

Table 1
A comparison of MRT LB models for local and nonlocal ACEs (M_t: mass of system, M_1: mass of phase 1, M_2: mass of phase 2, ϕ_{max}: maximum value of order parameter, ϕ_{min}: minimum value of order parameter).

	Local ACE	Nonlocal ACE	Initial solution (Eq. (49))
E	4.14237×10^{-4}	7.00748×10^{-4}	0
M_t	-1.01689×10^{4}	-1.01689×10^{4}	-1.01689×10^{4}
M_1	2.85581×10^{3}	2.85348×10^{3}	2.85693×10^{3}
M_2	-1.30247×10^{4}	-1.30224×10^{4}	-1.30258×10^{4}
ϕ_{max}	9.99998×10^{-1}	1	1
ϕ_{min}	-1	-1	-1

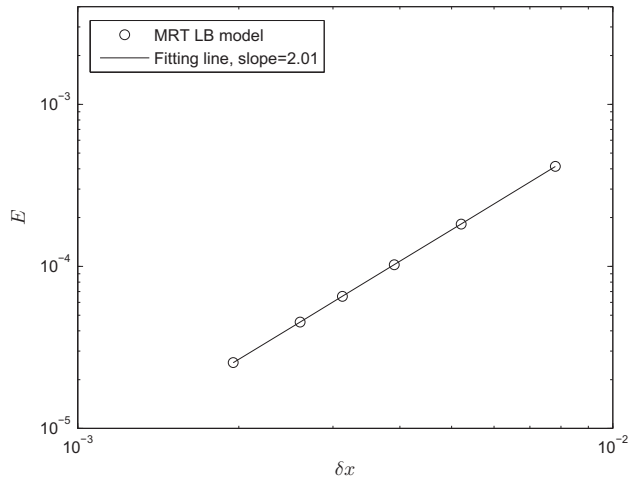

Fig. 2. Convergence rate of the MRT LB model for local ACE.

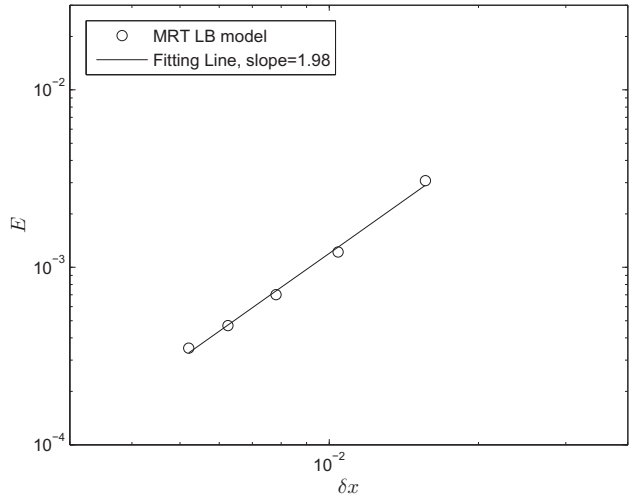

Fig. 3. Convergence rate of the MRT LB model for nonlocal ACE.

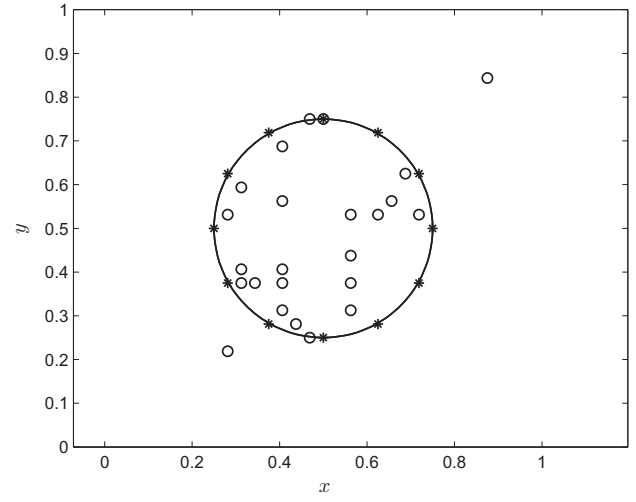

Fig. 4. The interface profiles of static disk (solid line: initial profile defined by Eq. (49), ○: local ACE, ∗: nonlocal ACE).

Table 2
A comparison of MRT LB models for local and nonlocal ACEs with a small lattice size (M_t: mass of system, M_1: mass of phase 1, M_2: mass of phase 2, ϕ_{max}: maximum value of order parameter, ϕ_{min}: minimum value of order parameter).

	Local ACE	Nonlocal ACE	Initial solution (Eq. (49))
E	2.84641×10^{-1}	3.0749×10^{-3}	0
M_t	-2.60697×10^{3}	-2.60697×10^{3}	-2.60697×10^{3}
M_1	2.84922×10^{2}	7.11881×10^{2}	7.14171×10^{2}
M_2	-2.89189×10^{3}	-3.31885×10^{3}	-3.32114×10^{3}
ϕ_{max}	9.77235×10^{-1}	1	1
ϕ_{min}	-9.96801×10^{-1}	-1	-1

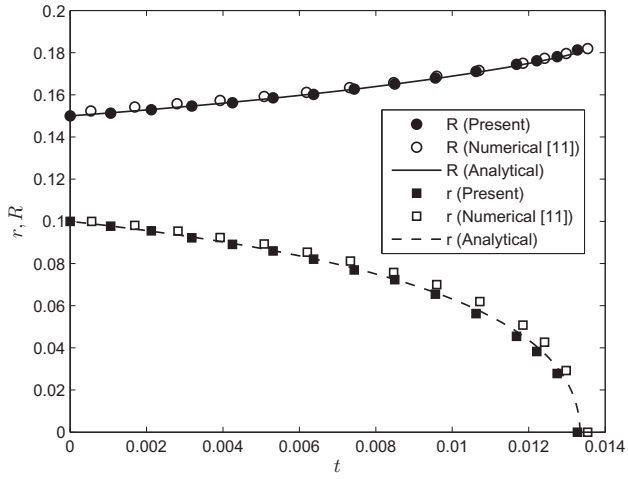

Fig. 5. The radii of two disks (R and r) at different time.

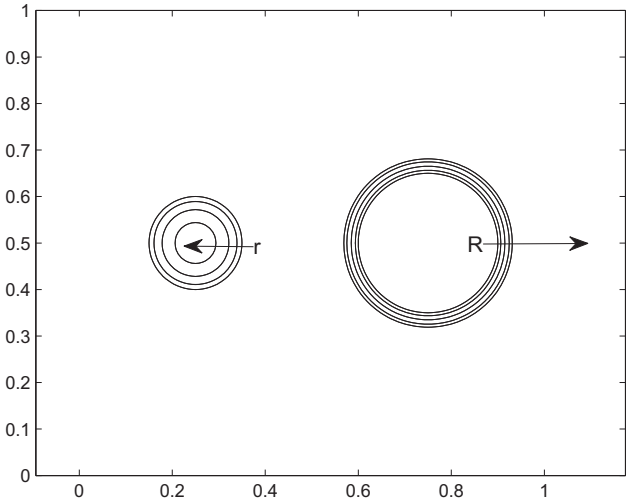

Fig. 6. The interface profiles of two disks (R and r) at different time.

tive errors of numerical results, the mass of phase 1, phase 2 and system, the maximum and minimum values of order parameter, and presented them in Table 1. As shown in this table, the local and nonlocal ACEs can guarantee the mass conservation of whole system, and the former is a little better in preserving mass conservation of each phase. However, compared to nonlocal ACE, the local ACE needs much more iteration steps to reach steady state where the numerical solution $\phi(x, y, t)$ satisfies the following relation,

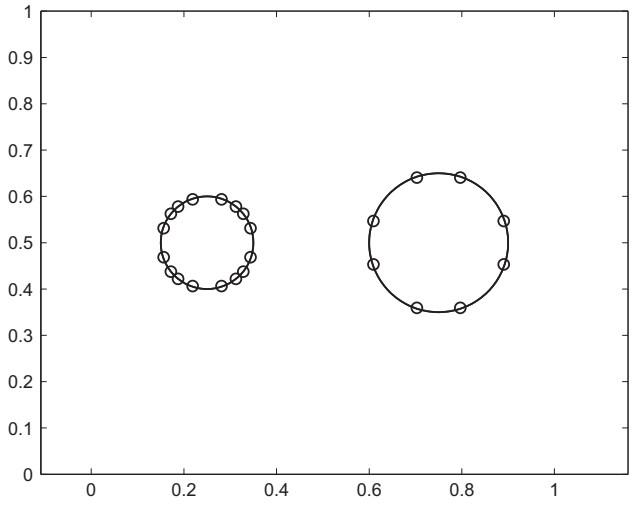

Fig. 7. The interface profiles of two disks at $t = 0$ and $t = T_{ext}$ (solid line: initial profile defined by Eq. (55), ∘: numerical results).

$$\frac{\sum_{(x,\,y)}|\phi(x,\,y,\,t)-\phi(x,\,y,\,t-100\times\delta t)|}{\sum_{(x,\,y)}|\phi(x,\,y,\,t)|}<5.0\times10^{-8}. \tag{50}$$

Actually, for the local ACE, the number of iterations needed to reach state is 4.13×10^4 (the CPU time is 1.794×10^2 s), while it is only 3.7×10^3 (the CPU time is 12.469 s) for local ACE. This may be because in the local ACE, the derivative term with a local characteristic is applied to preserve mass conservation, the integral term in nonlocal ACE, however, can be considered as a global characteristic in preserving mass conservation, and from numerical point of view, this global characteristic can also be used to accelerate the convergence of LB method. Besides, one can also find that the local ACE also brings some errors in predicting the maximum and minimum values of order parameter which would be more apparent with the decrease of lattice size.

Then this simple problem is also used to test the convergence rates of MRT LB models for local and nonlocal ACEs. To this end, we also carried out some simulations under different lattice sizes, and presented the relative errors in Figs. 2 and 3. From Fig. 2 where the lattice size is changed from 128×128 to 512×512, one can find that the MRT LB model for local ACE has a second-order convergence rate in space. Similarly, the MRT LB model for nonlocal ACE also has a second-order accuracy although its convergence rate is a little smaller than that of MRT LB model for local ACE, which can be seen clearly from Fig. 3 where the lattice size is varied from 64×64 to 192×192. On the other hand, since the nonlocal ACE only conserves mass of system up to ϵ^2 [41], the further increase of lattice size (larger than 192×192) cannot significantly improve accuracy of the numerical results. Actually, if we want to derive more accurate results with the MRT LB model for nonlocal ACEs, a smaller value of ϵ should be used, while a small ϵ may also bring instability problem since it leads to a small m.

Finally, from theoretical point of view, the MRT LB model for nonlocal ACE should be more stable than that for local ACE since the nonlocal integral term rather than local space derivative term is adopted to preserve the mass conservation. To conform this statement, a comparison of MRT LB models for local and nonlocal ACEs with a small lattice size 64×64 is conducted. Based on the results in Fig. 4 and Table 2 where the MRT LB model for local ACE is suspended at $T = 5\times10^6\delta t$ (the GPU time is 5.680×10^3 s) since it is difficult to obtain a steady and stable solution, while $T = 1.4\times10^3\delta t$ (the GPU time is 1.194 s) is enough for MRT LB model for nonlocal ACE to give a steady solution, one can find that the MRT LB model for nonlocal ACE can give a stable and accurate solution while the other one cannot.

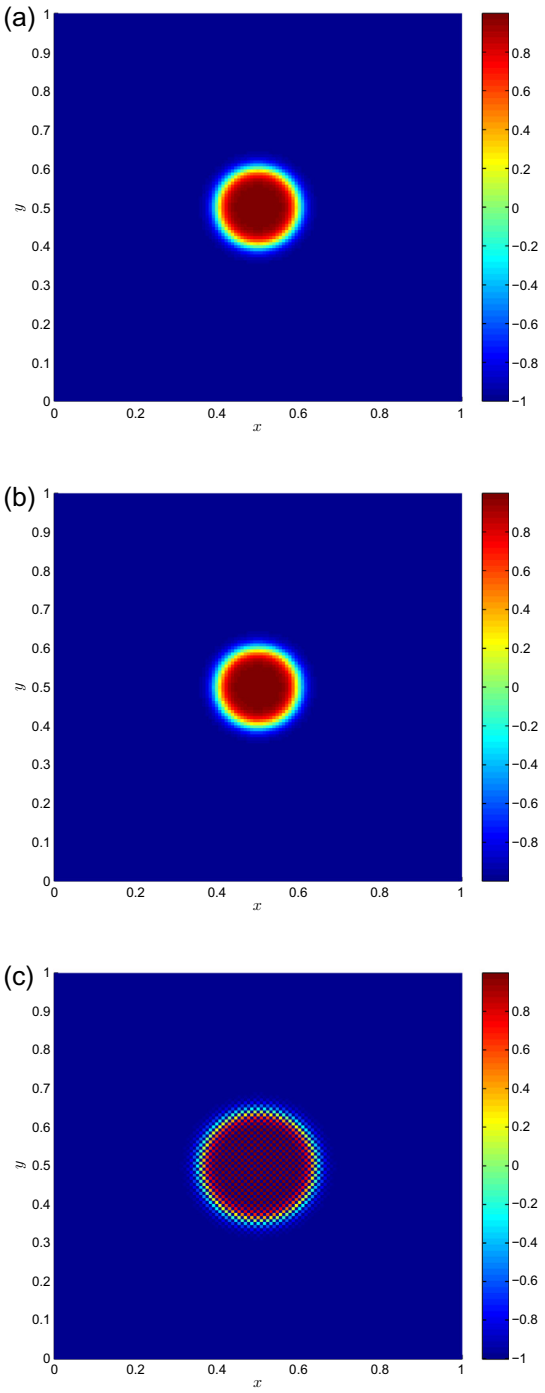

Fig. 8. Initial and numerical solutions of order parameter ϕ in the local and nonlocal ACEs ((a): Eq. (49), (b): local ACE, (c): nonlocal ACE).

4.2. Evolution of two disks

We further consider the evolution of two disks. If the interface based on nonlocal ACE ($M_\phi = 1.0$) approximates the motion by the volume-preserving mean curvature, the evolution law for radii of disks in two-dimensional space can be given by [11,14,41,70]

$$\frac{dr}{dt}=\frac{2}{r+R}-\frac{1}{r},\quad \frac{dR}{dt}=\frac{2}{r+R}-\frac{1}{R},\quad r<R, \tag{51}$$

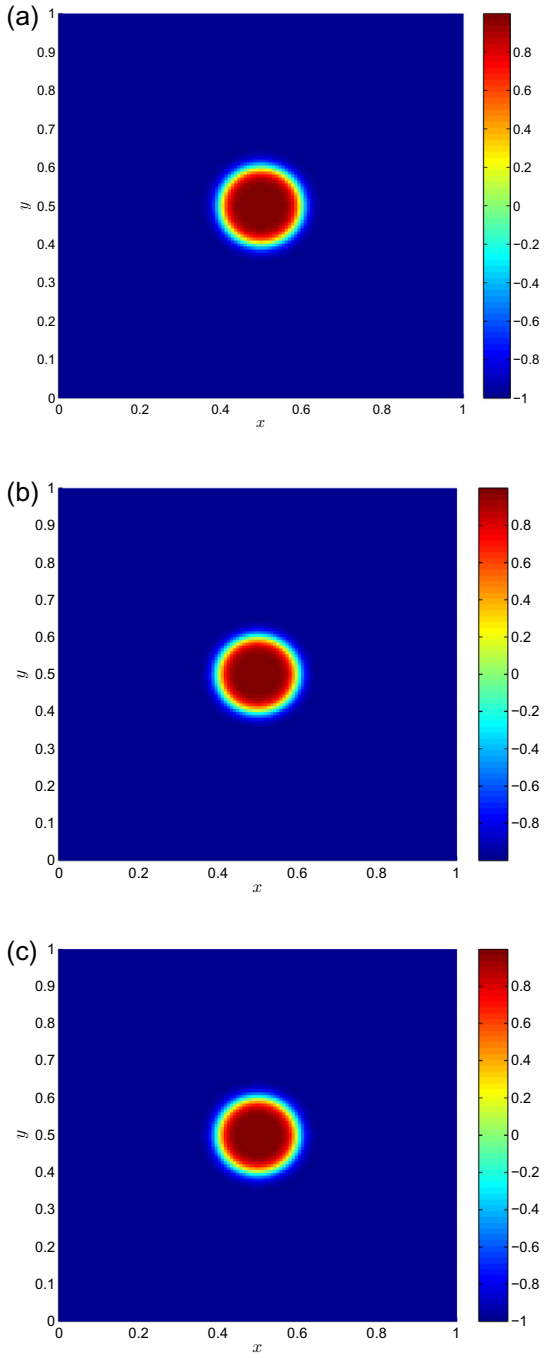

Fig. 9. Initial and numerical solutions of order parameter ϕ in the local and nonlocal ACEs ((a): Eq. (49), (b): local ACE, (c): nonlocal ACE).

where r and R are radii of two disks. Under the following initial conditions,

$$t = 0: \quad r = r_0, \quad R = R_0, \tag{52}$$

where r_0 and R_0 are two constants, one can obtain the analytical solutions of Eq. (51),

$$t = \frac{1}{2}\left\{ r\sqrt{R_m^2 - r^2} + R_m^2 \ln\left[\sqrt{1-\left(\frac{r}{R_m}\right)^2} - \frac{r}{R_m}\right] - \left(r_0 R_0 + R_m^2 \ln\frac{R_0 - r_0}{R_m}\right)\right\},$$
$$t = \frac{1}{2}\left\{ R\sqrt{R_m^2 - R^2} + R_m^2 \ln\left[\frac{R}{R_m} - \sqrt{1-\left(\frac{R}{R_m}\right)^2}\right] - \left(r_0 R_0 + R_m^2 \ln\frac{R_0 - r_0}{R_m}\right)\right\}, \tag{53}$$

$R_m = \sqrt{r_0^2 + R_0^2}$. Based on above analytical solutions, we can also determine the extinction time T_{ext} at which the smaller disk would disappear,

$$T_{ext} = \frac{1}{2}\left(R_m^2 \ln\frac{R_m}{R_0 - r_0} - r_0 R_0\right). \tag{54}$$

With the increase of time, the larger disk grows, and the radius can be increased up to the maximum value R_m.

The same as the previous work [11], here we also considered the case with $r_0 = 0.1$ and $R_0 = 0.15$ on the physical domain $\Omega = [0, 1] \times [0, 1]$, and determined the extinction time $T_{ext} = 0.01334$ from Eq. (54). We performed some simulations with the following initial condition,

$$\phi(x, y, 0) = \tanh\frac{R_0 - \sqrt{(x-0.75)^2 + (y-0.5)^2}}{\sqrt{2}\epsilon}, \quad x \geqslant 0.5, \tag{55a}$$

$$\phi(x, y, 0) = \tanh\frac{r_0 - \sqrt{(x-0.25)^2 + (y-0.5)^2}}{\sqrt{2}\epsilon}, \quad x < 0.5, \tag{55b}$$

and presented the results in Figs. 5 and 6 where $s_1 = 1.25$ and the lattice size is 128×128. As seen from these figures, the present results agree with the analytical solutions of Eq. (51), and they are also more accurate than numerical results in Ref. [11]. In addition, one can also find that the radius of larger disk increases with the increase of time, while the radius of smaller disk decreases in time, and reduces to zero at time $T = 0.01327$, which is a little smaller than the theoretical value $T_{ext} = 0.01334$.

When the MRT LB model for local ACE is used to investigate this problem, we can find that the numerical results agree well with initial solution (see Fig. 7), which means that during the time evolution, there are no apparent changes on the radii of two disks.

4.3. Small features

In this part, we would test the capacity of local and nonlocal ACEs in capturing small features. Here we still considered the problem of a static disk placed in the center of physical domain $\Omega = [0, 1] \times [0, 1]$, but the radius of the disk in the initial condition (49) is replaced by a small value $R = 0.1$. We noted that this problem has been studied in Ref. [14], and the results in this work also show that the original ACE and CH equations cannot preserve the circle shape of the disk, the disk would shrink during time evolution, and finally disappear at a certain time. However, the nonlocal ACE can keep the circle shape of the disk all the time.

We performed some simulations with the MRT LB models for local and nonlocal ACEs, and presented some results in Fig. 8 where the mobility, relaxation parameter and lattice size are set as $M_\phi = 0.001$, $s_1 = 1.25$ and 128×128. As shown in this figure, the numerical results of local ACE are close to its initial solution, but there are some great differences between the results of nonlocal ACE and initial solution which are mainly caused by the so-called checkerboard effect in LB method (see Fig. 8(c)) [71,72].

In the LB method, there are two possible ways that can be applied to eliminate this unphysical effect. The first one is that we can use the D2Q5 or D2Q9 lattice model instead of the D2Q4 lattice model to include rest particles. Actually, in the D2Q5 and D2Q9 lattice models, the populations at odd ($i + j = 2k + 1, k$ is a non-negative integer) and even ($i + j = 2k$) lattice points (i, j) are not independent since they are coupled through the rest particles [71], and thus the checkerboard effect can be removed. The other one is to change the lattice size used in our simulations [72]. For simplicity, here we adopted the latter approach, and used

Table 3
The effect of relaxation parameter s_1 on numerical results of local and nonlocal ACEs (M_t: mass of system, M_1: mass of phase 1, M_2: mass of phase 2, ϕ_{max}: maximum value of order parameter, ϕ_{min}: minimum value of order parameter).

Relaxation parameter s_1		Local ACE	Nonlocal ACE	Initial solution (Eq. (49))
$s_1 = 0.55$	E	5.06892×10^{-3}	7.00861×10^{-4}	0
	M_t	-1.01689×10^{4}	-1.01689×10^{4}	-1.01689×10^{4}
	M_1	2.83722×10^{3}	2.85348×10^{3}	2.85693×10^{3}
	M_2	-1.30061×10^{4}	-1.30224×10^{4}	-1.30258×10^{4}
	ϕ_{max}	9.99731×10^{-1}	1	1
	ϕ_{min}	-9.99945×10^{-1}	-1	-1
$s_1 = 0.75$	E	2.19708×10^{-3}	7.00839×10^{-4}	0
	M_t	-1.01689×10^{4}	-1.01689×10^{4}	-1.01689×10^{4}
	M_1	2.85099×10^{3}	2.85348×10^{3}	2.85693×10^{3}
	M_2	-1.30199×10^{4}	-1.30224×10^{4}	-1.30258×10^{4}
	ϕ_{max}	9.99891×10^{-1}	1	1
	ϕ_{min}	-9.99993×10^{-1}	-1	-1
$s_1 = 1.25$	E	4.14237×10^{-4}	7.00748×10^{-4}	0
	M_t	-1.01689×10^{4}	-1.01689×10^{4}	-1.01689×10^{4}
	M_1	2.85581×10^{3}	2.85348×10^{3}	2.85693×10^{3}
	M_2	-1.30247×10^{4}	-1.30224×10^{4}	-1.3026×10^{4}
	ϕ_{max}	9.99998×10^{-1}	1	1
	ϕ_{min}	-1	-1	-1
$s_1 = 1.75$	E	4.11612×10^{-4}	7.00209×10^{-4}	0
	M_t	-1.01689×10^{4}	-1.01689×10^{4}	-1.01689×10^{4}
	M_1	2.85582×10^{3}	2.85348×10^{3}	2.85693×10^{3}
	M_2	-1.30247×10^{4}	-1.30224×10^{4}	-1.30258×10^{4}
	ϕ_{max}	1	1	1
	ϕ_{min}	-1	-1	-1
$s_1 = 1.95$	E	4.098217×10^{-4}	6.97000×10^{-4}	0
	M_t	-1.01689×10^{4}	-1.01689×10^{4}	-1.01689×10^{4}
	M_1	2.85581×10^{3}	2.85348×10^{3}	2.85693×10^{3}
	M_2	-1.30247×10^{4}	-1.30224×10^{4}	-1.30258×10^{4}
	ϕ_{max}	1	1	1
	ϕ_{min}	-1	-1	-1

129×129 lattice size to replace the original one (128×128). From the results in Fig. 9, one can observe that the numerical results are in good agreement with the initial solution, and the relative errors of numerical results of local and nonlocal ACEs are 1.89831×10^{-4} and 4.36758×10^{-4}. These results also indicate that both the local and nonlocal ACEs can capture the small features of the system, but the local ACE is a little better than nonlocal ACE.

4.4. Effect of relaxation parameter

It is well known that the relaxation parameter s_1 in the LB method is a key physical parameter, and usually it also has a significant influence on the stability and accuracy of LB model [50,64–66]. Here we also adopted the problem of a static disk to test the effect of relaxation parameter s_1 on numerical results, and conducted some simulations with the same physical parameters appeared in Section 4.1. Based on the results in Table 3 where the lattice size is 128×128, one can observe that with the increase of relaxation parameter s_1, the numerical results of MRT LB model for the local ACE become more accurate, while it is interesting that the relaxation parameter s_1 has no apparent influence on the results of MRT LB model for the nonlocal ACE.

4.5. Effect of mobility

The mobility, as an important physical parameter in ACEs, may also affect the numerical results of present LB models. To test the effect of mobility, we also performed some simulations of a static disk with different values of mobility, and presented the results in Table 4 where the lattice size is 128×128, and the other parameters are the same as those appeared in Section 4.1. As seen from the table, the mobility almost has no influence on the results of MRT LB models for the local and nonlocal ACEs.

5. Conclusions

In this work, we first proposed two simple MRT LB models for local and nonlocal ACEs with the property of mass conservation, and also performed a detailed Chapman-Enskog analysis to show that the both the local and nonlocal ACEs can be exactly recovered from present MRT LB models. Then we conducted a comparative study of the local and nonlocal ACEs, and the numerical results show that although both local and nonlocal ACEs can guarantee the mass conservation of each phase and the whole system, the local ACE is more accurate than nonlocal ACE in preserving interface profile and mass conservation of each phase when the lattice size is fine enough. However, it is also found that the results of local ACE are dependent on the relaxation parameter s_1, and usually a larger relaxation parameter gives more accurate results. In addition, we also find that the nonlocal ACE is more stable than local ACE since the nonlocal integral term instead of the local space derivative term is adopted to preserve the mass conservation, and what is more, the numerical results of nonlocal ACE are almost independent of the relaxation parameter s_1.

Finally, considering the advantages of the ACE in depicting interfacial problems, the results presented in our work may be useful in the development of phased-field based LB models for multiphase flows.

Table 4
The effect of mobility M_ϕ on numerical results of local and nonlocal ACEs (M_t: mass of system, M_1: mass of phase 1, M_2: mass of phase 2, ϕ_{max}: maximum value of order parameter, ϕ_{min}: minimum value of order parameter).

Mobility M_ϕ		Local ACE	Nonlocal ACE	Initial solution (Eq. (49))
$M_\phi = 0.1$	E	4.14684×10^{-4}	7.00748×10^{-4}	0
	M_t	-1.01689×10^{4}	-1.01689×10^{4}	-1.01689×10^{4}
	M_1	2.85581×10^{3}	2.85348×10^{3}	2.85693×10^{3}
	M_2	-1.30247×10^{4}	-1.30224×10^{4}	-1.30258×10^{4}
	ϕ_{max}	9.99999×10^{-1}	1	1
	ϕ_{min}	-1	-1	-1
$M_\phi = 0.01$	E	4.14788×10^{-4}	7.00748×10^{-4}	0
	M_t	-1.01689×10^{4}	-1.01689×10^{4}	-1.01689×10^{4}
	M_1	2.85581×10^{3}	2.85348×10^{3}	2.85693×10^{3}
	M_2	-1.30247×10^{4}	-1.30224×10^{4}	-1.30258×10^{4}
	ϕ_{max}	9.99999×10^{-1}	1	1
	ϕ_{min}	-1	-1	-1
$M_\phi = 0.001$	E	4.14237×10^{-4}	7.00748×10^{-4}	0
	M_t	-1.01689×10^{4}	-1.01689×10^{4}	-1.01689×10^{4}
	M_1	2.85581×10^{3}	2.85348×10^{3}	2.85693×10^{3}
	M_2	-1.30247×10^{4}	-1.30224×10^{4}	-1.30258×10^{4}
	ϕ_{max}	9.99998×10^{-1}	1	1
	ϕ_{min}	-1	-1	-1
$M_\phi = 0.0001$	E	4.14638×10^{-4}	7.00748×10^{-4}	0
	M_t	-1.01689×10^{4}	-1.01689×10^{4}	-1.01689×10^{4}
	M_1	2.85581×10^{3}	2.85348×10^{3}	2.85693×10^{3}
	M_2	-1.30247×10^{4}	-1.30224×10^{4}	-1.30258×10^{4}
	ϕ_{max}	9.99999×10^{-1}	1	1
	ϕ_{min}	-1	-1	-1
$M_\phi = 0.00001$	E	4.14574×10^{-4}	7.00748×10^{-4}	0
	M_t	-1.01689×10^{4}	-1.01689×10^{4}	-1.01689×10^{4}
	M_1	2.85581×10^{3}	2.85348×10^{3}	2.85693×10^{3}
	M_2	-1.30247×10^{4}	-1.30224×10^{4}	-1.30258×10^{4}
	ϕ_{max}	9.99999×10^{-1}	1	1
	ϕ_{min}	-1	-1	-1

Conflict of interest

The authors declared that they have no conflicts of interest to this work.

Acknowledgments

This work was financially supported by the National Natural Science Foundation of China (Grant Nos. 51576079 and 51728601) and the National Key Research and Development Program of China (Grant No. 2017YFE0100100).

Appendix: Chapman-Enskog analysis

In this part, we would perform a Chapman-Enskog analysis to show how to derive the local and nonlocal ACEs from MRT LB models. In this classical analysis, the distribution function $f_i(\mathbf{x}, t)$, the derivatives of time and space, and the discrete source term R_i can be expanded as [47–50]

$$f_i = f_i^{(0)} + \varepsilon f_i^{(1)} + \varepsilon^2 f_i^{(2)} + \dots, \tag{56a}$$

$$\partial_t = \varepsilon\partial_{t_1} + \varepsilon^2\partial_{t_2}, \quad \nabla = \varepsilon\nabla_1 = (\partial_{x_1}, \partial_{y_1})^\top, \quad R_i = \varepsilon R_i^{(1)}, \tag{56b}$$

where ε is a small parameter.

Applying the Taylor expansion to Eq. (39), one can obtain

$$\delta t D_i f_i + \frac{\delta t^2}{2} D_i^2 f_i = -(\mathbf{M}^{-1}\mathbf{S}\mathbf{M})_{ij}\left[f_j - f_j^{(eq)}\right] + \delta t R_i, \tag{57}$$

where $D_i = \partial_t + \mathbf{c}_i \cdot \nabla$. Substituting Eq. (56) into Eq. (57) and dividing through by δt, one can derive the following equation,

$$\left[\varepsilon D_{i1} + \varepsilon^2\partial_{t_2} + \frac{\delta t}{2}\left(\varepsilon D_{i1} + \varepsilon^2\partial_{t_2}\right)^2\right]\left(f_i^{(0)} + \varepsilon f_i^{(1)} + \varepsilon^2 f_i^{(2)} + \dots\right) \tag{58}$$
$$= -(\mathbf{M}^{-1}\mathbf{S}'\mathbf{M})_{ij}\left[f_j^{(0)} + \varepsilon f_j^{(1)} + \varepsilon^2 f_j^{(2)} + \dots - f_j^{(eq)}\right] + \varepsilon R_i^{(1)},$$

where $D_{i1} = \partial_{t_1} + \mathbf{c}_i \cdot \nabla_1, \mathbf{S}' = \mathbf{S}/\delta t$.

From Eq. (58), we can obtain the zeroth, first and second-order equations in ε,

$$\varepsilon^0: \quad f_i^{(0)} = f_i^{(eq)}, \tag{59a}$$

$$\varepsilon^1: \quad D_{i1} f_i^{(0)} = -(\mathbf{M}^{-1}\mathbf{S}'\mathbf{M})_{ij} f_j^{(1)} + R_i^{(1)}, \tag{59b}$$

$$\varepsilon^2: \quad \partial_{t_2} f_i^{(0)} + D_{i1} f_i^{(1)} + \frac{\delta t}{2} D_{i1}^2 f_i^{(0)} = -(\mathbf{M}^{-1}\mathbf{S}'\mathbf{M})_{ij} f_j^{(2)}. \tag{59c}$$

To derive Eq. (59a), the relaxation matrix $\mathbf{S}$ has been assumed to be non-singular.

If we multiply the matrix $\mathbf{M}$ on both sides of Eqs. (59a)–(59c), we have

$$\varepsilon^0: \quad \mathbf{m}^{(0)} = \mathbf{m}^{(eq)}, \tag{60a}$$

$$\varepsilon^1: \quad \mathbf{D}_1\mathbf{m}^{(0)} = -\mathbf{S}'\mathbf{m}^{(1)} + \mathbf{Q}^{(1)}, \tag{60b}$$

$$\varepsilon^2: \quad \partial_{t_2}\mathbf{m}^{(0)} + \mathbf{D}_1\left(\mathbf{I} - \frac{\mathbf{S}}{2}\right)\mathbf{m}^{(1)} + \frac{\delta t}{2}\mathbf{D}_1\mathbf{Q}^{(1)} = -\mathbf{S}'\mathbf{m}^{(2)}, \tag{60c}$$

where Eq. (60b) has been adopted to obtain Eq. (60c). $\mathbf{m}^{(k)}=\mathbf{M}\mathbf{f}^{(k)}$ $(k=0,\ 1,\ \ldots)$ with $\mathbf{f}^{(k)}=\left(f_1^{(k)},\ \ldots,\ f_4^{(k)}\right)^{\top}$. Based on Eq. (60a), we can express $\mathbf{m}^{(0)},\mathbf{m}^{(1)}$ and $\mathbf{m}^{(2)}$ as

$$\mathbf{m}^{(0)}=(\phi,\ 0,\ 0,\ 0)^{\top},\ \mathbf{m}^{(1)}=\left(m_0^{(1)},\ m_1^{(1)},\ m_2^{(1)},\ m_3^{(1)}\right)^{\top},$$
$$\mathbf{m}^{(2)}=\left(0,\ m_1^{(2)},\ m_2^{(2)},\ m_3^{(2)}\right)^{\top}. \tag{61}$$

$\mathbf{D}_1=\partial_t\mathbf{I}+\mathbf{M}\mathrm{diag}(c_{1\alpha}\nabla_{1\alpha},\ \ldots,\ c_{4\alpha}\nabla_{4\alpha})\mathbf{M}^{-1}$, and $\mathbf{M}\mathrm{diag}(c_{1\alpha}\nabla_{1\alpha},\ \ldots,\ c_{4\alpha}\nabla_{4\alpha})\mathbf{M}^{-1}$ can also be determined explicitly by

$$\mathbf{M}\mathrm{diag}(c_{1\alpha}\nabla_{1\alpha},\ \ldots,\ c_{4\alpha}\nabla_{4\alpha})\mathbf{M}^{-1}=\begin{pmatrix}0 & \partial_x & \partial_y & 0\\ \frac{c^2}{2}\partial_x & 0 & 0 & \frac{1}{2}\partial_x\\ \frac{c^2}{2}\partial_y & 0 & 0 & -\frac{1}{2}\partial_y\\ 0 & c^2\partial_x & -c^2\partial_y & 0\end{pmatrix}. \tag{62}$$

$\mathbf{Q}^{(1)}=\mathbf{M}\mathbf{R}^{(1)}$ with $\mathbf{R}^{(1)}=\left(R_1^{(1)},\ \ldots,\ R_4^{(1)}\right)^{\top}$, which would be different in LB models for local and nonlocal ACEs, as seen below.

Appendix A. Chapman-Enskog analysis of LB model for local ACE

In the Chapman-Enskog analysis of LB model for local ACE, the discrete source term can be expanded as

$$R_i=\varepsilon R_i^{(1)}=\varepsilon\left[\mathbf{M}^{-1}\left(\mathbf{I}-\frac{\mathbf{S}}{2}\right)\mathbf{M}\right]_{ij}\omega_j\mathbf{c}_j\cdot\left(\frac{1-\phi^2}{\sqrt{2}\epsilon}\frac{\nabla_1\phi}{|\nabla_1\phi|}\right), \tag{63}$$

then one can determine $\mathbf{Q}_1^{(1)}$ as

$$\mathbf{Q}_1^{(1)}=\mathbf{M}\mathbf{R}^{(1)}=\frac{c^2}{2\sqrt{2}\epsilon}\frac{1-\phi^2}{|\nabla_1\phi|}\left[0,\ \left(1-\frac{s_1}{2}\right)\partial_{x_1}\phi,\ \left(1-\frac{s_1}{2}\right)\partial_{y_1}\phi,\ 0\right]^{\top}. \tag{64}$$

Based on Eqs. (25), (40) and (59a), one can obtain $m_0^{(1)}=0$. In addition, we can also obtain the first-order equations in ε from Eq. (60b), but for simplicity, only first three ones that would be used in the following analysis are given here,

$$\partial_{t_1}\phi=0, \tag{65a}$$

$$\frac{c^2}{2}\partial_{x_1}\phi=-\frac{1}{\delta t}s_1m_1^{(1)}+\frac{c^2}{2\sqrt{2}\epsilon}\frac{1-\phi^2}{|\nabla_1\phi|}\left(1-\frac{s_1}{2}\right)\partial_{x_1}\phi, \tag{65b}$$

$$\frac{c^2}{2}\partial_{y_1}\phi=-\frac{1}{\delta t}s_1m_2^{(1)}+\frac{c^2}{2\sqrt{2}\epsilon}\frac{1-\phi^2}{|\nabla_1\phi|}\left(1-\frac{s_1}{2}\right)\partial_{y_1}\phi. \tag{65c}$$

where Eqs. (61) and (62) have bee used.

With the help of Eqs. (65b) and (65c), one can derive the second-order equations in ε from Eq. (60c), and the first one corresponding to the conservative variable ϕ can be shown in the following form,

$$\partial_{t_2}\phi+\nabla_1\cdot\left[\frac{\delta t}{2}\left(\frac{1}{2}-\frac{1}{s_1}\right)c^2\left(1-\frac{1-\phi^2}{\sqrt{2}\epsilon}\frac{1}{|\nabla_1\phi|}\right)\nabla_1\phi\right]=0. \tag{66}$$

Through a combination of Eqs. (65a) and (66), i.e., $\varepsilon\times$ (65a) $+\varepsilon^2\times$ (66), we can exactly recover the local ACE (14) with M_ϕ defined by Eq. (46).

In addition, we also give some discussion on how to calculate the gradient term $\nabla\phi$. Actually, multiplying ε on both sides of Eqs. (65b) and (65c) yields

$$\frac{c^2}{2}\partial_x\phi=-\frac{1}{\delta t}s_1\left[m_1-m_1^{(0)}\right]+\frac{c^2}{2\sqrt{2}\epsilon}\frac{1-\phi^2}{|\nabla\phi|}\left(1-\frac{s_1}{2}\right)\partial_x\phi, \tag{67a}$$

$$\frac{c^2}{2}\partial_y\phi=-\frac{1}{\delta t}s_1\left[m_2-m_2^{(0)}\right]+\frac{c^2}{2\sqrt{2}\epsilon}\frac{1-\phi^2}{|\nabla\phi|}\left(1-\frac{s_1}{2}\right)\partial_y\phi, \tag{67b}$$

where the assumption $\varepsilon\mathbf{m}^{(1)}=\mathbf{m}-\mathbf{m}^{(0)}$ has been adopted [56,68]. Based on above two equations, one can first determine $|\nabla\phi|$ through solving a quadratic equation, but usually only one root of the quadratic equation is retained [35]. Then substituting the value $|\nabla\phi|$ into Eqs. (67a) and (67b), one can further obtain $\partial_x\phi$ and $\partial_y\phi$. To avoid the difficulties in solving quadratic equation, here we present a simple scheme to derive $\partial_x\phi$ and $\partial_y\phi$. We note that with the aid of Eq. (10) which has been used to obtain the local ACE (14), Eqs. (67a) and (67b) can be rewritten as

$$\frac{c^2}{2}\partial_x\phi=-\frac{1}{\delta t}s_1\left[m_1-m_1^{(0)}\right]+\frac{c^2}{2}\left(1-\frac{s_1}{2}\right)\partial_x\phi, \tag{68a}$$

$$\frac{c^2}{2}\partial_y\phi=-\frac{1}{\delta t}s_1\left[m_2-m_2^{(0)}\right]+\frac{c^2}{2}\left(1-\frac{s_1}{2}\right)\partial_y\phi, \tag{68b}$$

from which one can also obtain the following expressions of $\partial_x\phi$ and $\partial_y\phi$,

$$\partial_x\phi=-\frac{4}{\delta tc^2}m_1=-\frac{4}{\delta tc^2}\sum_i\mathbf{c}_{ix}f_i, \tag{69a}$$

$$\partial_y\phi=-\frac{4}{\delta tc^2}m_2=-\frac{4}{\delta tc^2}\sum_i\mathbf{c}_{iy}f_i, \tag{69b}$$

where $m_1^{(0)}=m_2^{(0)}=0$ has been used. Based on Eqs. (69a) and (69b), we can further determined $|\nabla\phi|$, as depicted by Eq. (42).

Appendix B. Chapman-Enskog analysis of LB model for nonlocal ACE

Following above analysis, the source term in the evolution equation of LB model for nonlocal ACE can be expanded as

$$R=\varepsilon R^{(1)}, \tag{70}$$

and consequently, $\mathbf{Q}^{(1)}$ can be given by

$$\mathbf{Q}^{(1)}=\mathbf{M}\mathbf{R}^{(1)}=\left[\left(1-\frac{s_0}{2}\right)R^{(1)},\ 0,\ 0,\ 0\right]^{\top}. \tag{71}$$

Similar to above discussion, with the aid of Eqs. (25), (45) and (59a), we can derive $m_0^{(1)}=-\delta tR^{(1)}/2$. From Eq. (60b), we can also obtain the first-order equations in ε, and express the first three ones as

$$\partial_{t_1}\phi=R^{(1)}, \tag{72a}$$

$$\frac{c^2}{2}\partial_{x_1}\phi=-\frac{1}{\delta t}s_1m_1^{(1)}, \tag{72b}$$

$$\frac{c^2}{2}\partial_{y_1}\phi=-\frac{1}{\delta t}s_1m_2^{(1)}, \tag{72c}$$

where Eqs. (61) and (62) have bee used.

Similarly, we can also derive the second-order equations in ε from Eq. (60c), and only present the first one here,

$$\partial_{t_2}\phi+\nabla_1\cdot\left[\frac{\delta t}{2}\left(\frac{1}{2}-\frac{1}{s_1}\right)c^2\nabla_1\phi\right]=0, \tag{73}$$

where Eqs. (72b) and (72c) have bee adopted. Combining Eqs. (72a) and (73), one can also recover the nonlocal ACE (22) with M_ϕ given by Eq. (46).

References

[1] D.M. Anderson, G.B. McFadden, A.A. Wheeler, Diffuse-interface methods in fluid mechanics, Annu. Rev. Fluid Mech. 30 (1998) 139–165.

[2] J. Shen, Modeling and numerical approximation of two-phase incompressible flows by a phase-field approach, in: W. Bao, Q. Du (Eds.), Multiscale Modeling and Analysis for Materials Simulation, IMS Lecture Notes Monogr. Ser. 9, IMS, Institute of Mathematical Statistics, Hayward, CA, 2011, pp. 147–196.
[3] J. Kim, Phase-field models for multi-component fluid flows, Commun. Comput. Phys. 12 (2012) 613–661.
[4] M. Wörner, Numerical modeling of multiphase flows in microfluidics and micro process engineering: a review of methods and applications, Microfluid. Nanofluid. 12 (2012) 841–886.
[5] H. Hua, J. Shin, J. Kim, Level set, phase-field, and immersed boundary methods for two-phase fluid flows, ASME J. Fluid Eng. 136 (2014) 021301.
[6] J.W. Cahn, J.E. Hilliard, Free energy of a non-uniform system I: interfacial free energy, J. Chem. Phys. 28 (1958) 258–267.
[7] S.M. Allen, J.W. Cahn, Mechanisms of phase transformations within the miscibility gap of Fe-rich Fe-Al alloys, Acta Metall. 24 (1976) 425–437.
[8] D. Jacqmin, Calculation of two-phase Navier-Stokes flows using phase-field modeling, J. Comput. Phys. 155 (1999) 96–127.
[9] D. Furihata, A stable and conservative finite difference scheme for the Cahn-Hilliard equation, Numer. Math. 87 (2001) 675–699.
[10] H. Lee, J. Kim, An efficient and accurate numerical algorithm for the vector-valued Allen-Cahn equations, Comput. Phys. Commun. 183 (2012) 2107–2115.
[11] J. Kim, S. Lee, Y. Choi, A conservative Allen-Cahn equation with a space-time dependent Lagrange multiplier, Int. J. Eng. Sci. 84 (2014) 11–17.
[12] S. Zhai, Z. Weng, X. Feng, Investigations on several numerical methods for the non-local Allen-Cahn equation, Int. J. Heat Mass Transf. 87 (2015) 111–118.
[13] Y. Li, J. Choi, J. Kim, Multi-component Cahn-Hilliard system with different boundary conditions in complex domains, J. Comput. Phys. 323 (2016) 1–16.
[14] D. Lee, J. Kim, Comparison study of the conservative Allen-Cahn and the Cahn-Hilliard equations, Math. Comput. Simul. 119 (2016) 35–36.
[15] J. Kim, D. Jeong, S.-D. Yang, Y. Choi, A finite difference method for a conservative Allen-Cahn equation on non-flat surfaces, J. Comput. Phys. 334 (2017) 170–181.
[16] S. Zhang, M. Wang, A nonconforming finite element method for the Cahn-Hilliard equation, J. Comput. Phys. 229 (2010) 7361–7372.
[17] J. Hua, P. Lin, C. Liu, Q. Wang, Energy law preserving C0 finite element schemes for phase field models in two-phase flow computations, J. Comput. Phys. 230 (2011) 7115–7131.
[18] C. Liu, J. Shen, A phase field model for the mixture of two incompressible fluids and its approximation by a Fourier-spectral method, Phys. D 179 (2003) 211–228.
[19] P. Yue, J.J. Feng, C. Liu, J. Shen, A diffuse-interface method for simulating two-phase flows of complex fluids, J. Fluid Mech. 515 (2004) 293–317.
[20] Y. He, Y. Liu, T. Tang, On large time-stepping methods for the Cahn-Hilliard equation, Appl. Numer. Math. 57 (2007) 616–628.
[21] H.W. Zheng, C. Shu, Y.T. Chew, Lattice Boltzmann interface capturing method for incompressible flows, Phys. Rev. E 72 (2005) 056705.
[22] A. Fakhari, M.H. Rahimian, Phase-field modeling by the method of lattice Boltzmann equations, Phys. Rev. E 81 (2010) 036707.
[23] Q. Li, K.H. Luo, Y.J. Gao, Y.L. He, Additional interfacial force in lattice Boltzmann models for incompressible multiphase flows, Phys. Rev. E 85 (2012) 026704.
[24] Y.Q. Zu, S. He, Phase-field-based lattice Boltzmann model for incompressible binary fluid systems with density and viscosity contrasts, Phys. Rev. E 87 (2013) 043301.
[25] H. Liang, B. Shi, Z.L. Guo, Z.H. Chai, Phase-field-based multiple-relaxation-time lattice Boltzmann model for incompressible multiphase flows, Phys. Rev. E 89 (2014) 053320.
[26] L. Zheng, S. Zheng, Q. Zhai, Lattice Boltzmann equation method for the Cahn-Hilliard equation, Phys. Rev. E 91 (2015) 013309.
[27] H. Liang, B.C. Shi, Z.H. Chai, Lattice Boltzmann modeling of three-phase incompressible flows, Phys. Rev. E 93 (2016) 013308.
[28] H. Liang, B.C.Q.X. Li, B.C. Shi, Z.H. Chai, Lattice Boltzmann simulation of three-dimensional Rayleigh-Taylor instability, Phys. Rev. E 93 (2016) 033113.
[29] K. Yang, Z. Guo, Lattice Boltzmann method for binary fluids based on mass-conserving quasi-incompressible phase-field theory, Phys. Rev. E 93 (2016) 043303.
[30] N. Wang, H. Liu, C. Zhang, Three-dimensional phase-field lattice Boltzmann model for incompressible multiphase flows, J. Comput. Sci. 17 (2016) 340–356.
[31] H. Liang, B.C. Shi, Z.H. Chai, An efficient phase-field-based multiple-relaxation-time lattice Boltzmann model for three-dimensional multiphase flows, Comput. Math. Appl. 73 (2017) 1524–1538.
[32] M. Geier, A. Fakhari, T. Lee, Conservative phase-field lattice Boltzmann model for interface tracking equation, Phys. Rev. E 91 (2015) 063309.
[33] A. Fakhari, M. Geier, Bolster, A simple phase-field model for interface tracking in three dimensions, Comput. Math. Appl. https://doi.org/10.1016/j.camwa.2016.08.021.
[34] F. Ren, B. Song, M.C. Sukop, H. Hu, Improved lattice Boltzmann modeling of binary flow based on the conservative Allen-Cahn equation, Phys. Rev. E 94 (2016) 023311.
[35] H.L. Wang, Z.H. Chai, B.C. Shi, H. Liang, Comparative study of the lattice Boltzmann models for Allen-Cahn and Cahn-Hilliard equations, Phys. Rev. E 94 (2016) 033304.
[36] P. Yue, C. Zhou, J.J. Feng, Spontaneous shrinkage of drops and mass conservation in phase-field simulations, J. Comput. Phys. 223 (2007) 1–9.
[37] L. Zheng, T. Lee, Z. Guo, D. Rumschitzki, Shrinkage of bubbles and drops in the lattice Boltzmann equation method for nonideal gases, Phys. Rev. E 89 (2014) 033302.
[38] Y. Sun, C. Beckermann, Sharp interface tracking using the phase-field equation, J. Comput. Phys. 220 (2007) 626–653.
[39] P.-H. Chiu, Y.-T. Lin, A conservative phase field method for solving incompressible two-phase flows, J. Comput. Phys. 230 (2011) 185–204.
[40] J. Rubinstein, P. Sternberg, Nonlocal reaction-diffusion equations and nucleation, IMA J. Appl. Math. 48 (1992) 249–264.
[41] M. Brassel, E. Bretin, A modified phase field approximation for mean curvature flow with conservation of the volume, Math. Meth. Appl. Sci. 34 (2011) 1157–1180.
[42] X. Yang, J.J. Feng, C. Liu, J. Shen, Numerical simulations of jet pinching-off and drop formation using an energetic variational phase-field method, J. Comput. Phys. 218 (2006) 417–428.
[43] Z. Zhang, H. Tang, An adaptive phase field method for the mixture of two incompressible fluids, Comput. Fluids 36 (2007) 1307–1318.
[44] D. Jeong, J. Kim, conservative Allen-Cahn-Navier-Stokes system for incompressible two-phase flows, Comput. Fluids 156 (2017) 239–246.
[45] R. Folch, J. Casademunt, A. Hernández-Machado, Phase-field model for Hele-Shaw flows with arbitrary viscosity contrast. I. Theoretical approach, Phys. Rev. E 60 (1999) 1724–1733.
[46] M. Alfaro, P. Alifrangis, Convergence of a mass conserving Allen-Cahn equation whose Lagrange multiplier is nonlocal and local, Int. Free Bound. 16 (2014) 243–268.
[47] S. Chen, G. Doolen, Lattice Boltzmann method for fluid flows, Annu. Rev. Fluid Mech. 30 (1998) 329–364.
[48] S. Succi, The Lattice Boltzmann Equation for Fluid Dynamics and Beyond, Oxford University Press, Oxford, 2001.
[49] Z. Guo, C. Shu, Lattice Boltzmann Method and Its Applications in Engineering, World Scientific, Singapore, 2013.
[50] T. Krüger, H. Kusumaatmaja, A. Kuzmin, O. Shardt, G. Silva, E.M. Viggen, The Lattice Boltzmann Method: Principles and Practice, Springer, Switzerland, 2017.
[51] A. Xu, W. Shyy, T.S. Zhao, Lattice Boltzmann modeling of transport phenomena in fuel cells and flow batteries, Acta Mech. Sin. 33 (2017) 555–574.
[52] A. Xu, G.-C. Zhang, Y.-B. Gan, F. Chen, X.-J. Yu, Lattice Boltzmann modeling and simulation of compressible flows, Front. Phys. 7 (2012) 582–600.
[53] D. Sun, M. Zhu, J. Wang, B. Sun, Lattice Boltzmann modeling of bubble formation and dendritic growth in solidification of binary alloys, Int. J. Heat Mass Transf. 94 (2016) 474–487.
[54] I. Ginzburg, Equilibrium-type and link-type lattice Boltzmann models for generic advection and anisotropic-dispersion equation, Adv. Water Resour. 28 (2005) 1171–1195.
[55] B. Shi, Z. Guo, Lattice Boltzmann model for nonlinear convection-diffusion equations, Phys. Rev. E 79 (2009) 016701.
[56] Z. Chai, B. Shi, Z. Guo, A multiple-relaxation-time lattice Boltzmann model for general nonlinear anisotropic convection-diffusion equations, J. Sci. Comput. 69 (2016) 355–390.
[57] U. Frisch, B. Hasslacher, Y. Pomeau, Lattice-Gas Automata for the Navier-Stokes equation, Phys. Rev. Lett. 56 (1986) 1505–1508.
[58] X. He, L.-S. Luo, Theory of the lattice Boltzmann method: from the Boltzmann equation to the lattice Boltzmann equation, Phys. Rev. E 56 (1997) 6811–6817.
[59] Y.H. Qian, D. d'Humières, P. Lallemand, Lattice BGK models for Navier-Stokes equation, Europhys. Lett. 17 (1992) 479–484.
[60] I. Ginzburg, F. Verhaeghe, D. d'Humières, Two-relaxation-time lattice Boltzmann scheme: about parametrization, velocity, pressure and mixed boundary conditions, Commun. Comput. Phys. 3 (2008) 427–478.
[61] D. d'Humières, Generalized lattice-Boltzmann equations, in: B.D. Shizgal, D.P. Weave (Eds.), Rarefied Gas Dynamics: Theory and Simulations, Prog. Astronaut. Aeronaut, vol. 159, AIAA, Washington, DC, 1992, pp. 450–458.
[62] P. Lallemand, L.-S. Luo, Theory of the lattice Boltzmann method: dispersion, dissipation, isotropy, Galilean invariance, and stability, Phys. Rev. E 61 (2000) 6546–6562.
[63] C. Pan, L.-S. Luo, C.T. Miller, An evaluation of lattice Boltzmann schemes for porous medium flow simulation, Comput. Fluids 35 (2006) 898–909.
[64] L.-S. Luo, W. Liao, X. Chen, Y. Peng, W. Zhang, Numerics of the lattice Boltzmann method: effects of collision models on the lattice Boltzmann simulations, Phys. Rev. E 83 (2011) 056710.
[65] S. Cui, N. Hong, B. Shi, Z. Chai, Discrete effect on the halfway bounce-back boundary condition of multiple-relaxation-time lattice Boltzmann model for convection-diffusion equations, Phys. Rev. E 93 (2016) 043311.
[66] Z. Chai, C. Huang, B. Shi, Z. Guo, A comparative study on the lattice Boltzmann models for predicting effective diffusivity of porous media, Int. J. Heat Mass Transf. 98 (2016) 687–696.
[67] H. Yoshida, M. Nagaoka, Multiple-relaxation-time lattice Boltzmann model for the convection and anisotropic diffusion equation, J. Comput. Phys. 229 (2010) 7774–7795.
[68] Z. Chai, T.S. Zhao, Nonequilibrium scheme for computing the flux of the convection-diffusion equation in the framework of the lattice Boltzmann method, Phys. Rev. E 90 (2014) 013305.
[69] Z. Chai, T.S. Zhao, Lattice Boltzmann model for the convection-diffusion equation, Phys. Rev. E 87 (2013) 063309.
[70] L. Bronsard, B. Stoth, Volume-preserving mean curvature flow as a limit of a nonlocal Ginzburg-Landau equation, SIAM J. Math. Anal. 28 (1997) 769–807.
[71] D. Kandhai, A. Koponent, A. Hoekstra, M. Kataja, J. Timonen, P.M.A. Sloot, Implementation aspects of 3D lattice-BGK: boundaries, accuracy, and a new fast relaxation method, J. Comput. Phys. 150 (1999) 482–501.
[72] Z. Guo, B. Shi, C. Zheng, Chequerboard effects on spurious currents in the lattice Boltzmann equation for two-phase flows, Phil. Trans. R. Soc. A 369 (2011) 2231–2283.